Detection of GNSS Ionospheric Scintillations based on Machine Learning Decision Tree

This article has been accepted for publication in a future issue of this journal, but has not been fully edited. Content may change prior to final publication. Citation information: DOI 10.1109/TAES.2018.2850385, IEEE Transactions on Aerospace and Electronic Systems

Detection of GNSS Ionospheric Scintillations based on Machine Learning Decision Tree

Nicola Linty, Alessandro Farasin, Alfredo Favenza, and Fabio Dovis

Abstract

This paper proposes a methodology for automatic, accurate and early detection of amplitude ionospheric scintillation events, based on machine learning algorithms, applied on big sets of 50 Hz post-correlation data provided by a GNSS receiver. Experimental results on real data show that this approach can considerably improve traditional methods, reaching a detection accuracy of 98%, very close to human-driven manual classification. Moreover, the detection responsiveness is enhanced, enabling early scintillation alerts.

Keywords

Ionospheric scintillations, Machine learning, GNSS.

I. Introduction

The propagation through the atmosphere has a significant influence on radio signals broadcast by satellites towards the Earth. Irregularities and gradients of the ionization of the upper layer of the atmosphere, the ionosphere, a region characterized by a high concentration of free electrons, can cause fluctuations of the signal amplitude and phase, which are called *ionospheric scintillations*. Scintillations also affect Global Navigation Satellite System (GNSS) trans-ionospheric signals. Under disturbed ionospheric conditions, GNSS receivers are more subject to phase errors, cycle slips, increased carrier Doppler jitter and losses of lock, resulting in positioning errors of the order of tens of meters, and, in the most severe cases, even in the complete receiver outage [1]. Scintillations are a threat to GNSSs since they may have disruptive impact on the user receiver performance when high accuracy, reliability and continuity of the positioning service are needed, as for example for critical applications and precise positioning [2]–[4].

As a consequence, scintillation monitoring and detection is a key aspect for improving the quality and reliability of GNSS observations [5]. Networks of GNSS receivers, specifically designed for accomplishing these tasks, have been installed in recent years, both at low and high latitudes, where scintillation is more likely to occur [6], [7]. The purpose is indeed twofold: on one side, observation of the signals themselves, which are a source of information for understanding and modeling the upper layers of the atmosphere [8]; on the other side, the signals can be used as detectors and triggers to raise warning and take countermeasures for GNSS-based operations. For this reason, it is important to design receivers robust to the presence of scintillation, but also to have proper algorithms for the detection of the event and its classification [9].

Nicola Linty and Fabio Dovis are with the Department of Electronics and Telecommunications (DET), Politecnico di Torino, Italy (e-mail: nicola.linty@polito.it; fabio.dovis@polito.it).

Alessandro Farasin and Alfredo Favenza are with the Istituto Superiore Mario Boella (ISMB), Torino, Italy (e-mails: alessandro.farasin@ismb.it, alfredo.favenza@ismb.it).

Early and accurate detection of scintillation events is a very important feature for space weather applications, for atmospheric remote sensing and in general for all those data collection systems that automatically detect and record Intermediate Frequency (IF) raw samples [10], [11]. However, the scientific literature about scintillation detection techniques is limited. Most of the works are based on very simple event triggers, which are based on the comparison of scintillation indices provided by commercial receivers with preset threshold values [12]. However, this approach overlooks high moment characteristics of the signals and requires detrending operations. Some alternatives to traditional scintillation indices were proposed, for instance exploiting wavelet techniques [13], decomposing the Carrier-to-Noise density power ratio (C/N_0) by means of adaptive time-frequency methods [14] of evaluating statistical properties of the histogram of received samples [15]. The common drawback of such techniques is that they rely on complex and computationally expensive operations or on dedicated receiver architectures.

Recent studies have demonstrated that machine learning techniques can be exploited for scintillation detection. In [16], the authors propose a survey of data mining techniques, relying on observation and integration of GNSS receivers, other sensors and online forecast services. However, this approach relies on external data sources and instruments, which are not always available. A technique based on supervised machine learning Support Vector Machine (SVM) algorithm has been proposed for amplitude scintillation detection in [17] and [18]. This method has been extended to phase scintillation detection in [19] and [20]. The main limitations of these approaches are: they provide a detection trigger at a low rate; they are based on SVM models, which are computationally demanding; and they have been tested on a set of data pre-filtered at an elevation mask of 30°, thus discarding potentially useful and important data.

The work presented in this paper aims at proposing an alternative method for the detection of amplitude scintillation based on machine learning. The scope of this approach is multifold:

- to propose an alternative to the use of traditional scintillation indices, the performance of which may depend on algorithmic choices, such as detrending and average operations;
- to use only common GNSS stand-alone receivers observables;
- to be able to understand the presence of the scintillation event including the transient time before and after its strongest phase, thus providing an early run-time alert;
- to provide an automatic method, resembling manual observation of the observables, while keeping the cost low in terms of human effort and enabling run-time detection;
- to reduce the rate of false alarms due to the ambiguity between scintillation and other events, such as multipath, that may affect the assessment of the classical amplitude scintillation index, without the need of pre-filtering data;
- to reduce the missed detection caused by a-priori filtering of data at low elevation angle, often implemented to hard-cut multipath effect;
- to use computationally efficient machine learning algorithms, such decision tree.

The paper is organized as follows. After this introduction, which has outlined the scope of the work, Section II provides an overview on scintillation, its effects on GNSS signals and applications, and on machine learning algorithms, models and metrics for performance evaluation. Section III gives an overview of traditional scintillation detection techniques and analyzes their limitations on selected case studies. Section IV introduces machine learning detection, identifying two different sets of features based on different receiver measurements. Section V validates the proposed approaches, presenting quantitative and qualitative results obtained running

different machine learning algorithms on different sets of features. Finally, Section VI draws conclusions and outlines the future work.

II. General overview

This section presents a general overview on GNSS, ionospheric scintillation and machine learning. A reader expert in the field can skip to Section III.

A. GNSS and ionospheric scintillations

GNSSs are radio-communication satellite systems that enable a generic user to compute Position, Velocity and Time (PVT) at its current location, anywhere on the Earth, processing Radio Frequency (RF) signals transmitted from a constellation of satellites and performing trilateration with respect to the satellites, taken as reference points [21]. Despite being originally developed for localization, GNSSs are not limited to positioning purposes, but span an unlimited range of applications, including scientific observations.

One of the main characteristic of GNSS signals is their low received power. For this reason, the accuracy, availability and reliability of the position solution is threatened by potential errors, affecting the overall quality of the process. Ionospheric propagation is the major and more variable natural error source in GNSS signal processing at the receiver level. Propagation through this layer introduces a potentially strong degradation of the GNSS signal, as depicted in Fig. 1, causing significant errors in any GNSS-based application. The ionosphere affects the quality of GNSS signals both in terms of a temporal delay and of scintillations. While delay compensation techniques are nowadays applied in any GNSS receiver [21], scintillations is still an issue for both mass-market and professional devices. Occurrence of scintillations is very difficult to be modeled, due to their quasi-random nature [22]. Therefore, they remain, to this day, one of the major limiting factors for high accuracy applications.

Scintillation monitoring is indeed a central activity, both in the GNSS and in the space weather community. The amount of scintillation affecting a satellite signal can be evaluated by exploiting the correlation output values. Two indices are usually considered: S_4 for amplitude scintillation and σ_ϕ for phase scintillation. S_4 measures the amount of amplitude fluctuations due to scintillations in GNSS signals; it corresponds to the normalized standard deviation of the detrended Signal Intensity (SI) computed from the in-phase (I) and quadrature-phase (Q) prompt correlation samples. σ_ϕ is calculated as the standard deviation of the detrended carrier phase measurements. Both indices are calculated over a varying observation interval, usually equal to 60 seconds.

Most of the works on scintillation monitoring are based on the comparison of the value of these two indices with predefined thresholds. Nevertheless, detection based on such fixed thresholds can be misleading, due to: the loss of the transient phases of the events, causing a delay in the raise of possible warning flags; the missed detection of weak events with high variance; or the signal distortions caused by other phenomena, such as multipath. The only reliable procedure is to entrust the detection of scintillation events to a human-driven visual inspection of data.

B. Machine learning

Machine learning [23] is the systematic study of intelligent algorithms and systems that improve their knowledge or performance by experience. In its general concept, machine learning process (Fig. 2) refers to the ability of solving a task, processing right features describing the domain of interest, according to a

This article has been accepted for publication in a future issue of this journal, but has not been fully edited. Content may change prior to final publication. Citation information: DOI 10.1109/TAES.2018.2850385, IEEE Transactions on Aerospace and Electronic Systems

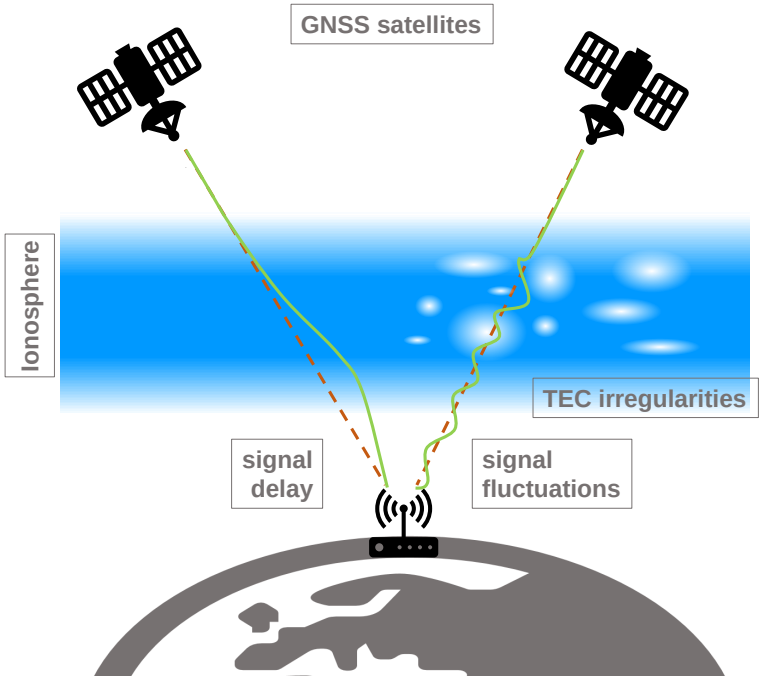

Fig. 1. Pictorial representation of ionospheric delay and scintillation phenomena. The red dashed lines are the line-of-sight signal paths from the GNSS satellites to the receiver on earth; the green continuous signal accounts for propagation distortions.

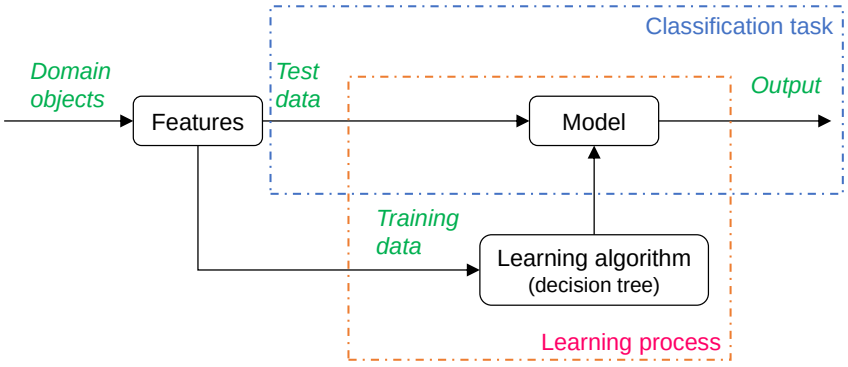

Fig. 2. Flow diagram of the machine learning process. In the first stage, the learning process, depicted in the red box, a model is defined, using training data, selected features and a specific learning algorithm, such as a decision tree. The model is then applied on the test dataset in the classification task, in the blue box, to generate the output.

model. The use of machine learning in Location Based Services (LBS) is also motivated by the increasing volume of available data collected at remote sites through low cost GNSS software receivers [24].

The problem under investigation in this work is a typical binary classification task that can be undertaken exploiting a machine learning approach on a big data set. The main elements of machine learning are [25]:

- *domain*, the problem to be solved (detection of ionospheric scintillation events in GNSS data collections);
- *features*, the description of the objects of the domain (GNSS observables);
- *task*, the abstract representation of the problem which reflects in the mapping between the input and the output (the automatic classification of data collection sample in scintillation/non-scintillation);
- *model*, the output of the machine learning when the training set is fed to the algorithms.

This article has been accepted for publication in a future issue of this journal, but has not been fully edited. Content may change prior to final publication. Citation information: DOI 10.1109/TAES.2018.2850385, IEEE Transactions on Aerospace and Electronic Systems

The machine learning goal is to identify the right algorithm, or set of algorithms, to use the right set of features to build the right models that achieve the right tasks in terms of detection accuracy. This goal is achieved by feeding the machine learning algorithms with two different sets of data:

- a *training-set* of historical, pre-labeled data;
- a *test-set*, non-labeled, possibly real-time data.

Machine learning offers a large number of algorithms, to build models from a given dataset of input observations, and to make predictions and decision expressed as output. These algorithms are mainly grouped under three big families:

- supervised learning, where input data (training set) has a known label or result;
- unsupervised learning, where input data is not labeled and does not have a known result;
- semi-supervised learning, where input data is a mixture of labeled and unlabeled examples.

Since the goal of this research is classification of data on the basis of the detection of scintillation events and the input training set is fully labeled, this study will take into consideration two types of supervised learning algorithms: decision tree and random forest.

1) Decision Tree: Decision tree is one of the most commonly used classification technique [26]. It is based on tree structures, defined by recursively partitioning the input space: each internal node represents a certain feature of the domain; each branch, emanating from the node, is the outcome of the decision taken in the node according to a function; and each leaf represents a final classification decision, corresponding to the conjunction of single decisions taken during on the path from the root of the tree to the leaf. The learning takes place as the machine creates a set of rules defining a model, in terms of sequence of the features along the branches and functions for the decision criteria in each node. The rules are based on the concept of *utility* of a feature for the classification purpose.

Lets consider two classes, D^+ and D^-, and a boolean feature, D_1, which can take the values D_1^+ and D_1^-. The ideal situation is when $D_1^+ = D^+$ and $D_1^- = \emptyset$, or $D_1^+ = \emptyset$ and $D_1^- = D^-$: in this case, the branches are said to be pure. Typically this situation never happens, so the task is to measure the impurity of each feature and corresponding function. Extending the problem to a general case, the goal is to measure the impurity of a set of n^+ positives and n^- negatives, in terms of empirical probability $\dot{p} = n^+/(n^+ + n^-)$, to evaluate the best rule. A cost function is defined to achieve this task, thus building the tree model. Among several possibilities, such as the minority class or the Gini index, the *entropy* $\mathcal{E}$ was chosen:

$$\mathcal{E} = -\dot{p}\log_2(\dot{p}) - (1-\dot{p})\log_2(1-\dot{p}) \tag{1}$$

By minimizing the entropy, the information gain brought by the tree is maximized. Further mathematical details on decisions trees can be found in [23], [27], [28].

2) Random Forest: Random forest is an ensemble learning method for classification, based on the construction of a multitude of decision trees at training time [29]. It helps to overcome the problem of overfitting, as well as to reduce the variance of an estimate, exploiting averaging. Random forests are a combination of tree predictors such that each tree depends on the values of a random vector sampled independently and with the same distribution for all trees in the forest. The generalization error for forests converges to a limit as the number of trees in the forest becomes large and depends on the strength of the individual trees in the forest and the correlation between them.

This article has been accepted for publication in a future issue of this journal, but has not been fully edited. Content may change prior to final publication. Citation information: DOI 10.1109/TAES.2018.2850385, IEEE Transactions on Aerospace and Electronic Systems

3) Performance evaluation metrics: Performance of a machine learning classification algorithm is typically evaluated using statistical tools and metrics [28]. One of the most common is the confusion matrix, or contingency table; an example is reported in TABLE I. Each row refers to actual classes as annotated in the test case, each column to classes as predicted by the classifier. Last column and last row give the marginals, which are important to allow the statistical significance assessment. In order to distinguish performance on the classes, correctly classified positives and negatives are referred to as True Positives and True Negatives, respectively; incorrect classified positives are called False Negatives or missed detections; misclassified negatives are called False Positives, or false alarms. Consequently, the True positive rate is the proportion of positives correctly classified, also called sensitivity or recall, while the True negative rate is the proportion of negatives correctly classified.

TABLE I. GENERAL EXAMPLE OF A CONFUSION MATRIX.

		Prediction	
		0	1
Truth	0	True negatives	False positives
	1	False negatives	True positives

Other metrics that can be used to assess the machine learning performance are:

- *Accuracy*: the percentage of correct predictions made by the model over a data set, calculated as: $\text{True Positives} + \text{True Negatives}$.
- *Precision*: the ratio of correct positive observations, calculated as: $\text{True Positives}/\left(\text{True Positives} + \text{False Positives}\right)$.
- *Recall*: the ratio of correctly predicted positive events, also known as sensitivity, calculated as: $\text{True Positives}/\left(\text{True Positives} + \text{False Negatives}\right)$.
- *F-score*: an alternative measure of a test accuracy, taking into account also both false positives and false negatives. It corresponds to the weighted average of Precision and Recall: $\left(2 \cdot \text{Recall} \cdot \text{Precision}\right) / \left(\text{Recall} + \text{Precision}\right)$.

4) k-fold cross validation: Cross-validation is a validation technique which measures how the results of a statistical analysis will generalize to an independent dataset. In fact, knowledge about the test-set can affect the model and the evaluation metrics decreasing generalization performance. This situation is typically called overfitting. A solution to this problem is a procedure called cross-validation. In the basic approach adopted in this paper, denoted k-fold cross validation [30], the training set is split into k smaller sets, called folds. Afterwards, for each of the k folds, first a model is trained, using the remaining $k-1$ folds as training data. The resulting model is then used to test the untrained fold. Finally, the average of the values obtained in each iteration is computed.

III. TRADITIONAL SCINTILLATION DETECTION

In this section, the traditional state-of-the-art approaches for amplitude scintillation detection are presented. Two detection rules are considered and tested on two case studies, evaluating and carefully discussing their performance and limitations.

A. Description of traditional methods

The majority of the works on amplitude scintillation monitoring are based on the analysis of the value of the S_4 index. Scintillation is typically considered present if S_4 exceeds a predefined threshold $\mathcal{T}_{S_4}$. Different detection rules can be identified, according to the literature on the topic.

1) Hard detection: A Hard detection rule is defined by simply applying the threshold $\mathcal{T}_{S_4}$ on the estimated value of S_4. Ionospheric scintillation is present at epoch n if and only if:

$$S_4\left[n\right] > \mathcal{T}_{S_4} \tag{2}$$

It is a simple approach, easy to be implemented, but it might lead to an undesired and non-negligible number of false alarms. The threshold is commonly assumed to be $\mathcal{T}_{S_4} = 0.4$ by many authors [31]–[35]; other works consider scintillation moderate in the range between 0.2 and 0.5, and strong above 0.5 [36].

As the S_4 index is a measure of the variation of the amplitude of the GNSS signal, it is not unlikely that events other than ionospheric scintillation cause it to increase above the threshold, in a way similar to what scintillations do, thus affecting the detection process. This is particularly frequent for low elevation satellites, when the number of multipath reflected rays increases and, at the same time, the C/N_0 is lower.

2) Semi-hard detection: In order to better characterize the scintillation phenomenon and to reduce the false alarm rate, more filters can be applied to the signal. For example, it is quite common to apply an elevation mask; most of the multipath-induced false alarms can be removed by considering only signals from satellites above a certain elevation angle. Further conditions can be defined on the C/N_0 value, so as to exclude noisy measurements, or on the satellites azimuth ϑ_{az}. According to the Semi-hard detection rule, scintillation is present at epoch n if and only if:

$$S_4\left[n\right] > \mathcal{T}_{S_4} \quad \wedge \quad \theta_{\mathrm{el}}\left[n\right] > \mathcal{T}_{\theta_{\mathrm{el}}} \quad \wedge \quad C/N_0\left[n\right] > \mathcal{T}_{C/N_0} \tag{3}$$

The value of the elevation threshold $\mathcal{T}_{\theta_{\mathrm{el}}}$ is typically set to 30° [36], [37]. The definition of $\mathcal{T}_{C/N_0}$ is more complex, as the C/N_0 is the result of an estimation process and depends on the receiver implementation. The value $37\ \mathrm{dBHz}$ gives satisfactory results [38]. Nevertheless, it has been proven that the filter on the C/N_0 is not very discriminant in terms of detection results; lower values, such as $30\ \mathrm{dBHz}$, which corresponds to the sensitivity of a standard tracking loop, lead to analog results.

3) Manual detection: A "third" approach corresponds to human-driven manual and subjective identification of the portion of data affected by scintillation. This can be achieved by visual inspection of the S_4 and C/N_0 estimates, of the satellite azimuth and elevation and of the comparison of historical data. Even though this approach lacks scientific rigor, it can assure the best detection performance, provided that the person doing the manual annotation has enough knowledge and experience. However, it is time-consuming, subject to human errors and not automatic.

In this paper, the manual annotation is considered as the reference *ground truth* for the detection performance analysis. The same approach has been used also in other works relying on machine learning for scintillation detection [17], [18].

B. Case studies

The examples refer to GNSS data collections performed on March 26 and April 2, 2015, in Hanoi (Vietnam), at $11^\circ\ 20'$ N geo-magnetic latitude, using a customized Software Defined Radio (SDR)-based GNSS data grabber and software receiver [38]. Moderate and strong amplitude scintillation events were observed; the Dst index

This article has been accepted for publication in a future issue of this journal, but has not been fully edited. Content may change prior to final publication. Citation information: DOI 10.1109/TAES.2018.2850385, IEEE Transactions on Aerospace and Electronic Systems

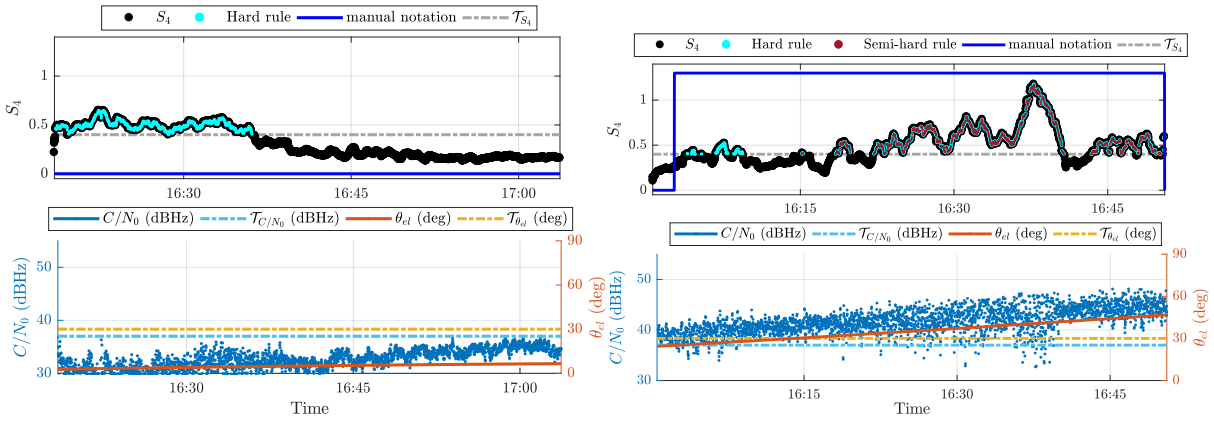

(a) April 2, PRN 23

(b) March 26, PRN 10

Fig. 3. Comparison of traditional scintillation detection methods for two different scintillation events. Top panels report the trend of the S_4, the manual annotation, the detection results of the Hard and Semi-hard rules and the value of the S_4 threshold $\mathcal{T}_{S_4} = 0.4$. Bottom panels report the elevation and C/N_0 trends, and their respective thresholds used in traditional rules, $\mathcal{T}_{\theta_{\text{el}}} = 30°$ and $\mathcal{T}_{C/N_0} = 37$ dBHz.

negative peaks, provided by the World Data Center of Kyoto, amount to -20 nT and -21 nT respectively. Global Positioning System (GPS) L1 C/A signals are considered, respectively of Pseudo-Random Noise (PRN) satellite 10 and 23. Fig. 3 shows the estimates of the S_4 index (top plot, black dots), of the C/N_0 and of the satellite elevation (bottom plot, blue and red lines respectively) as computed by the software receiver. In addition, three horizontal lines are drawn in correspondence of the S_4, C/N_0 and elevation thresholds, used in the detection rules.

Traditional detection rules for scintillation monitoring are applied.

1) All points for which scintillation is detected according to the Hard rule, (2), are colored in cyan. In this case, $\mathcal{T}_{S_4} = 0.4$; therefore, all points with a S_4 higher than 0.4 are marked as scintillation.
2) All points for which scintillation is detected according to the Semi-hard rule, (3), are colored in magenta. In this case, $\mathcal{T}_{\theta_{\text{el}}} = 30°$ and $\mathcal{T}_{C/N_0} = 37$ dBHz; as a consequence, only a subset of points of the previous case are marked as scintillation.
3) All points enclosed by the blue boxes are manually marked as scintillation by visual inspection.

From a careful analysis of the figure, it is clear that the Hard and Semi-Hard rules fail in identifying scintillation, when compared to the manual annotation, considered as ground truth. In particular, in the first case, reported in Fig. 3a, the high S_4 values in the time interval between 16:18 and 16:36 are likely due to multipath reflections. This is evident by considering the fact that the satellite is rising (elevation lower than $5°$), but also exploiting a-priori information on environmental conditions, such as the presence of obstacles in the satellite line-of-sight, or historical data analysis, such as the sidereal repetition of the event with the same S_4 pattern. The detection results of the Hard rule are then characterized by a high false alarm rate. On the contrary, the Semi-hard rule correctly marks all the points as no scintillation, thanks to the filter added by the threshold on the elevation.

On the other hand, in the second case, depicted in Fig. 3b, both rules are too conservative. There are time windows which are part of the same scintillation event, but the values of S_4 and θ_{el} slightly lower than the corresponding thresholds classify them as non scintillated time epochs, thus generating a high missed detection rate. The interval from 16:03 to 16.20 is the leading edge phase of the event detected starting from 16:20. Similarly, the interval from 16:40 to 16:44 can be considered scintillation, even if the S_4 value is slightly below

This article has been accepted for publication in a future issue of this journal, but has not been fully edited. Content may change prior to final publication. Citation information: DOI 10.1109/TAES.2018.2850385, IEEE Transactions on Aerospace and Electronic Systems

the detection threshold; the presence of high S_4 values a few minutes before and after this time interval assures that it can be marked as scintillation.

Results can be formalized by means of the confusion matrix. In the first example, no scintillation is present, so the False Positives and False Negatives are equal to 0. While the semi-hard rule gives a True negatives rate of 100%, this percentage reduces to 61.6% for the Hard rule. In the second example, the rate of True negatives and False positives is the same for both rules, and corresponds to 4.2% and 0% respectively. However, in this case the Hard rule has a True positives rate of almost 58%, overcoming the Semi-hard (51.8%), which in turn has a higher False positives rate.

The overall confusion matrices for detection results of the two examples and for both the Hard and Semi-hard rule are reported in TABLE II. The Hard rule detection gives an overall percentage of correct estimations of only $32.9\% + 29\% = 61.9\%$. The false alarm rate amounts to 19.2%, while the missed detection rate is 18.1%. When moving to the Semi-hard case, the number of points correctly estimated increases to $52.1\% + 25.9\% = 78\%$. As expected, the false alarms are 0%, but the missed detection rate increases to 22%.

TABLE II. CONFUSION MATRICES FOR THE HARD AND SEMI-HARD RULE, ON THE EXAMPLES OF MARCH 26, PRN 10 AND APRIL 2, PRN 23.

C. Limitations

As demonstrated by the previous examples, the traditional thresholding-based approaches for automatic scintillation detection appear not to be able to fully characterize the event, since decisions based on hard thresholds do not take into account either the physics of the event, or the environmental conditions. Multipath, interference and other nuisances might lead to erroneous scintillation detection, as S_4 overlooks the higher-moments characteristics of the signals.

Furthermore, it has to be remarked that the computation of S_4 is cumbersome and demanding: it requires complex averaging and detrending operations on the correlation outputs, in order to reduce noise and to remove the slow variations due to the signal dynamics. The choice of the best detrending technique is not trivial: several approaches, based on the use of high-order Butterworth filters, of wavelet transformations, and on simple averaging, have been described [39]–[41]. Nevertheless, it has been proven that different methods lead to different results [42]. It has also been proven that a different detrending shall be chosen for different geographical areas [43] and that detrending operations could introduce post-processing artifacts [19].

Manual annotation can assure higher accuracy in the event classification, in terms of duration and continuity, at the expenses of a time-consuming human-driven visual inspection. Furthermore it is a post-processing analysis which is not suitable for a quasi real-time detection. As a summary, strengths and weaknesses of these three approaches are reported in TABLE III.

This article has been accepted for publication in a future issue of this journal, but has not been fully edited. Content may change prior to final publication. Citation information: DOI 10.1109/TAES.2018.2850385, IEEE Transactions on Aerospace and Electronic Systems

TABLE III. SUMMARY OF THE TRADITIONAL SCINTILLATION DETECTION APPROACHES STRENGTHS AND WEAKNESSES.

Detection	Strengths	Weaknesses
Hard	Very simple rule. Easy implementation also in real time.	Low detection accuracy Requires detrending. False alarms due to multipath reflections.
Semi-hard	Increased accuracy. Higher robustness to non-ionospheric impairments.	Not general approach. Location dependent. Higher computational burden.
Manual	High accuracy. Cross analysis of historical data.	Costly and time consuming. Dependent on human experience. Subjected to human errors. Non-real-time (post-processing).

This, in turn, justifies the investigation of different detection and classification techniques. The limitations of the aforementioned approaches can be mitigated exploiting machine learning techniques, able to learn from human processes to produce automatic high accuracy detection and classification.

IV. MACHINE LEARNING SCINTILLATION DETECTION

The goal of the machine learning detection algorithm is to replicate the performance of the manual detection, without introducing additional human effort to manually classify the data. The algorithm, once trained on big datasets labeled by manual annotation, demonstrates better detection properties with respect to the Hard and Semi-hard approaches.

The machine learning algorithm considered is the *decision tree*, as it offers the best compromise between computational complexity, performance and data pre-processing operations. k-fold cross validation, with $k = 10$, is performed on the dataset: for each run, 90% of input data are used in the training phase and 10% of data are used for the test set.

A. Correlation matrix analysis and features selection

The first necessary step is the selection of the features used to train the model. Features shall be selected between the measurements provided by a GNSS receiver. Nevertheless, their choice is not trivial, and the final performance of the algorithm, as well as the scalability and generality of the technique, depend on the features chosen.

The correlation matrix is a statistical tool used to underline the correlation between each couple of features. Each cell of the correlation matrix reports the Pearson correlation coefficient between variables X and Y, defined as:

$$\rho\left(X,Y\right)=\frac{\sigma_{XY}}{\sigma_X\sigma_Y}=\frac{\sum_{i=1}^{n}\left(x_i-\bar{x}\right)\left(y_i-\bar{y}\right)}{\sqrt{\sum_{i=1}^{n}\left(x_i-\bar{x}\right)^2}\sqrt{\sum_{i=1}^{n}\left(y_i-\bar{y}\right)^2}} \tag{4}$$

where x_i is a single record of the dataset and $\bar{x}$ is the sample mean. The correlation coefficient ranges from -1 to 1. Correlation between X and Y is absent when the correlation coefficient $\rho\left(X,Y\right)$ is equal to 0, weak when $|\rho\left(X,Y\right)|\leq 0.35$, moderate in the range 0.36 to 0.67 and strong when it exceeds 0.68 [44].

This article has been accepted for publication in a future issue of this journal, but has not been fully edited. Content may change prior to final publication. Citation information: DOI 10.1109/TAES.2018.2850385, IEEE Transactions on Aerospace and Electronic Systems

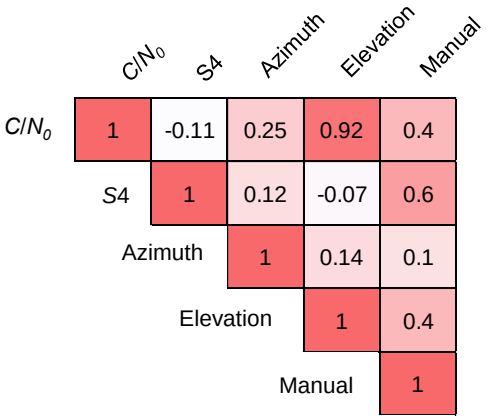

Fig. 4. Correlation matrix, considering the observables of the signal.

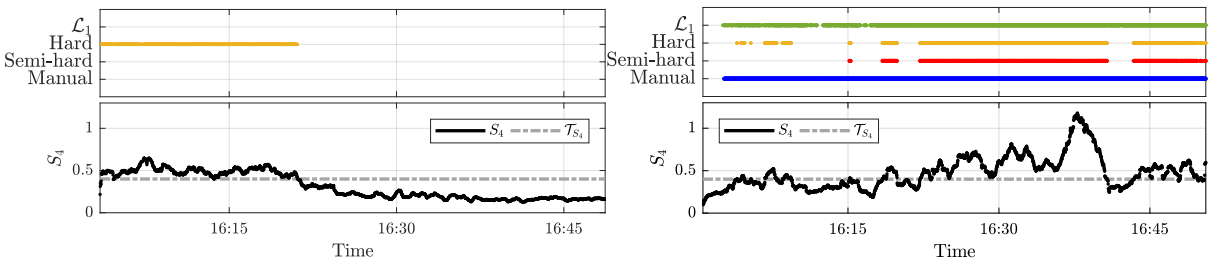

(a) April 2, PRN 23

(b) March 26, PRN 10

Fig. 5. Decision tree detection results for two different scintillation events and for set $\mathcal{L}_1$. Top panels report the manual annotation (ground truth), the detection results of the Hard and Semi-hard rules, and the machine learning detection results. Bottom panels report the trend of the S_4 and the value of the S_4 threshold $\mathcal{T}_{S_4} = 0.4$.

B. Observable-based features

Fig. 4 reports the matrix of the correlation $\rho\,(X, Y)$ between the manual ground truth and the 1 Hz observables provided by the GNSS scintillation monitoring receiver: S_4, C/N_0, θ_{el} and ϑ_{az}. Manual annotation has a moderate correlation with C/N_0, θ_{el} and S_4, and a very low correlation with ϑ_{az}.

A first set of features, $\mathcal{L}_1$, that looks to be a reasonable starting choice, is then defined as:

$$\mathcal{L}_1 = \{S_4,\, C/N_0,\, \theta_{\mathrm{el}}\} \tag{5}$$

It includes the observables having the highest correlation with the manual annotation. Furthermore, they are the same parameters used in the Semi-hard detection rule (3).

The same two case studies considered in Section III-B are analyzed. The detection results of machine learning algorithm based on set $\mathcal{L}_1$ are reported in Fig. 5, along with the detection results of the Hard and Semi-hard rules. The blue line identifies the manual human-driven detection. The green line corresponds to the detection results of the machine learning decision tree algorithm. With respect to the Hard and Semi-hard cases, and compared to the manual detection, machine learning results show both a lower rate of false alarms, in the example of Fig. 5a, and a lower rate of missed detection, in the example of Fig. 5b.

The confusion matrix, reported in TABLE IV, summarizes the results. When compared to the case reported in Fig. 3, the missed detection rate is reduced to 7.4%, while there are no false alarms. The global success rate corresponds to $52.1\% + 40.5\% = 92.6\%$, meaning that for more than 9 cases over 10 the machine learning

This article has been accepted for publication in a future issue of this journal, but has not been fully edited. Content may change prior to final publication. Citation information: DOI 10.1109/TAES.2018.2850385, IEEE Transactions on Aerospace and Electronic Systems

prediction matches the manual annotation. It is important to underline that these two examples, in particular the first, reflect a *worst case* situation, in which the presence of multipath introduces a further level of complexity. More simple cases, relative to portions of the dataset affected by scintillation only, show a higher success rate, and are not reported here.

TABLE IV. CONFUSION MATRIX FOR MACHINE LEARNING PREDICTION AND FOR THE SET $\mathcal{L}_1$, ON THE EXAMPLES OF MARCH 26, PRN 10 AND APRIL 2, PRN 23.

		Prediction	
		0	1
Manual	0	52.1	0
	1	7.4	40.5

Nevertheless, although the results in terms of scintillation detection are good, the approach based on the signal observables reveals some limitations. On one side, the use of S_4 should be avoided, as it already corresponds to the output of the traditional approach. In addition, its derivation is computationally demanding and involves complex operations that could introduce post-processing artifacts and location dependent solutions. At the same time, the use of C/N_0 could lead to misleading detection result, as, in the presence of scintillation, it might be affected by a bias or even provide completely wrong results [18]. Finally, the use of satellites elevation can potentially lead to overfitting, making the model suitable only for the specific location of the data collection used for the training.

C. Signal-based features

In order to further improve the machine leargning scintillation detection performance, it is possible to exploit, as features, not the final observables and the final scintillation index, but rather their components; in other words, to unpack the S_4 formulation [45]. In this section the raw GNSS signal measurements at the output of the receiver tracking stage in time domain are used as features, the 50 Hz I and Q correlators output. They correspond to the higher rate observables which can be provided by a commercial receiver, and thus to the most accurate representation of the original GNSS signal. It will be proven that a machine learning approach that uses raw observables as features rather than the scintillation indices not only is able to detect scintillations, but offers a higher performance. Furthermore, such an approach overtakes the problem of computing the scintillation indices and is able to exclude the side effects and artifacts introduced by the post-processing.

I and Q values cannot be directly injected in the learning, but they have to be averaged, in order to reduce the impact of thermal noise and to highlight the scintillation phenomenon. Therefore new quantities are defined, based on a short observation window, T_{obs}. N samples of I and Q are averaged over the observation period, where $N = T_{\text{obs}} \cdot 50$ Hz. The averaged correlations samples, denoted $\langle I \rangle$ and $\langle Q \rangle$, are then defined as:

$$\langle I \rangle = \frac{1}{N} \sum_{n=1}^{N} I_n \tag{6}$$

$$\langle Q \rangle = \frac{1}{N} \sum_{n=1}^{N} Q_n \tag{7}$$

This article has been accepted for publication in a future issue of this journal, but has not been fully edited. Content may change prior to final publication. Citation information: DOI 10.1109/TAES.2018.2850385, IEEE Transactions on Aerospace and Electronic Systems

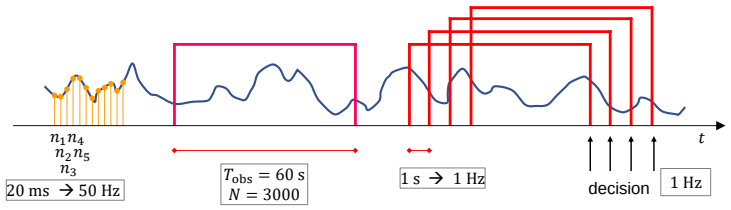

Fig. 6. Illustration of the samples averaging and window overlapping procedure used in the work.

where I_n and Q_n are respectively the I and Q correlator outputs at time n.

In order to combine the information brought by phase and quadrature components, the SI, at time n, can be computed:

$$SI_n = I_n^2 + Q_n^2 \tag{8}$$

Similarly, SI is averaged over the observation period:

$$\langle SI \rangle = \frac{1}{N} \sum_{n=1}^{N} SI_n = \frac{1}{N} \sum_{n=1}^{N} \left(I_n^2 + Q_n^2 \right) \tag{9}$$

This suggests to compute other two additional features, i.e. the average over the observation period of the square of the I and Q correlators:

$$\left\langle I^2 \right\rangle = \frac{1}{N} \sum_{n=1}^{N} I_n^2 \tag{10}$$

$$\left\langle Q^2 \right\rangle = \frac{1}{N} \sum_{n=1}^{N} Q_n^2 \tag{11}$$

By analogy with the previous cases and with the algorithm used to compute S_4, a last feature is identified as the average over the observation windows of the square of the SI:

$$\left\langle SI^2 \right\rangle = \frac{1}{N} \sum_{n=1}^{N} SI_n^2 \tag{12}$$

A new subset of features, including combinations of the I and Q correlators, is introduced:

$$\mathcal{L}_2 = \left\{ \langle I \rangle, \langle Q \rangle, \langle SI \rangle, \left\langle I^2 \right\rangle, \left\langle Q^2 \right\rangle, \left\langle SI^2 \right\rangle \right\} \tag{13}$$

On the other hand, previous works on the topic consider as a feature only the Fourier transform of the SI [19], [20]. Furthermore, it is important to mention that, contrary to what is typically done in literature [18], [46], no prior elevation-based filtering aiming at reducing the effect of multipath is performed. Indeed, applying a mask partially hides the signal distortion phenomenon that are under study.

The features in (13) are obtained by averaging $N = 3000$ values of the 50 Hz correlator stage outputs. The observation windows is set to $T_{\text{obs}} = 60$ s, in agreement with common scintillation observation algorithms [22]. In addition, a sliding and overlapping windowing technique is applied, depicted in Fig. 6: by shifting the observation window of 1 s, the resolution of the observation is increased to 1 Hz. The same average operation over 60 s of values is performed and a set of new features is injected in the machine learning algorithm at the end of each window, thus at a 1 Hz rate.

The correlation matrix for the set of features $\mathcal{L}_2$ is reported in Fig. 7. From the table, it emerges that a moderate correlation is experienced between the manual scintillation annotation and the variables $\langle SI \rangle$, $\left\langle I^2 \right\rangle$ and $\left\langle SI^2 \right\rangle$.

This article has been accepted for publication in a future issue of this journal, but has not been fully edited. Content may change prior to final publication. Citation information: DOI 10.1109/TAES.2018.2850385, IEEE Transactions on Aerospace and Electronic Systems

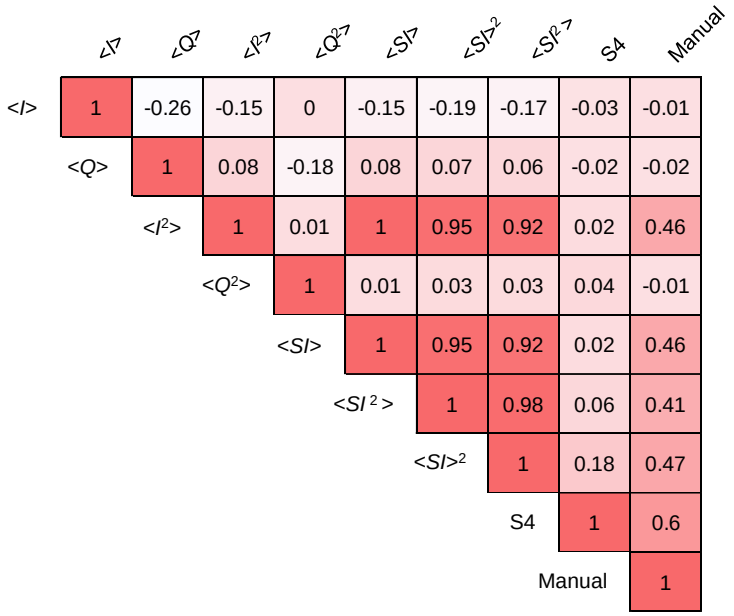

Fig. 7. Correlation matrix considering the features defined in set $\mathcal{L}_2$.

The results obtained running decision tree on set $\mathcal{L}_2$ on the selected case studies will be presented in Section V-B, respectively in Fig. 11a and 11b.

V. Results

In this section, a complete performance analysis of different machine learning algorithms, on the full dataset, and considering different sets of features, is provided and compared to the traditional detection methods. First, quantitative results in terms of confusion matrices, accuracy, precision, recall and F-score are reported and commented. Then qualitative results focusing on the punctual analysis of some false negatives and false positives predictions are proposed, with a focus on the run time detection capabilities. To conclude, results of a test on novel, untrained data, collected in a different location, are presented.

Data are part of the same data collection described in Section III-B (Hanoi, Vietnam, at $11^\circ\,20'$ N geomagnetic latitude, in March and April 2015). They include a total of 169 955 entries of data at 50 Hz resolution, spanning a total time interval of about 6 hours, and including in total 20 different satellites. The rate of scintillation events is about 1:4.

A. Quantitative results

1) Hard and Semi-hard rules: First, summary results related to the Hard and Semi-hard rules tests are reported. The confusion matrices are depicted in TABLE V. The number of false positives and of false negatives is quite high in both cases, respectively 18.75% and 13.87%. In the Semi-hard rule case, the percentage of false positives is reduced to only 0.26%, at the expenses of a higher rate of false negatives. This is justified recalling that the Semi-hard rule is a conservative approach.

Accuracy, precision, recall and F-score are reported in the first two rows of TABLE VI. Although also precision and recall are reported, a fair performance analysis shall be made focusing on the the accuracy, and in particular on the F-score. As detailed in Section II-B3, precision and recall give a partial overview on

This article has been accepted for publication in a future issue of this journal, but has not been fully edited. Content may change prior to final publication. Citation information: DOI 10.1109/TAES.2018.2850385, IEEE Transactions on Aerospace and Electronic Systems

TABLE V. CONFUSION MATRICES FOR THE HARD AND SEMI-HARD RULE, ON THE COMPLETE DATASET.

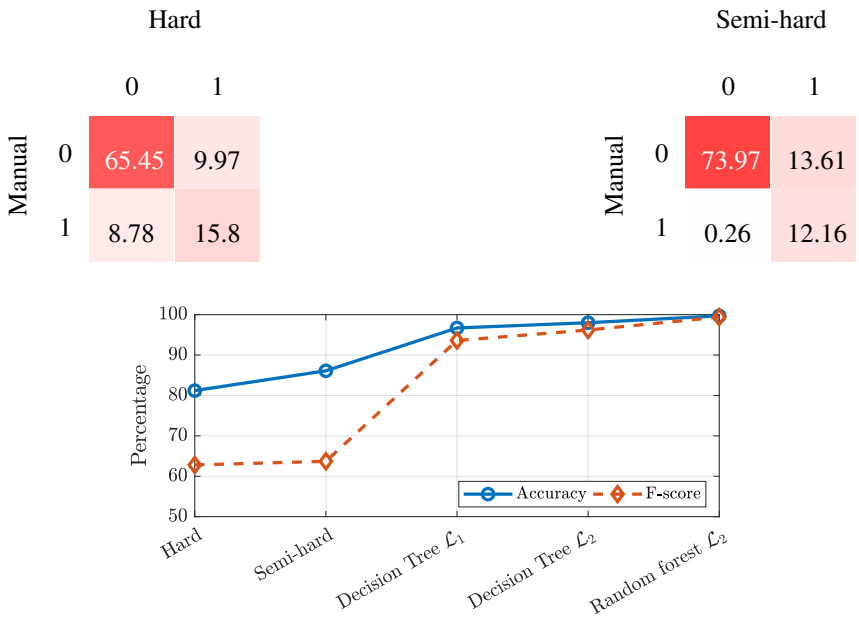

Fig. 8. Summary of the accuracy and F-score obtained for the different scintillation detection techniques presented.

the goodness of the algorithms, while the F-score is the most complete metric, taking into account also the numerosity of the points denoted as scintillated. The accuracy is about 5% higher in the second case. However, the lower value of the recall is the sign of an uneven evaluation of the performance. Indeed, the F-score for the two approaches is similar; the Semi-hard algorithm only improves this indicator by 1%. The two approaches can then be defined similar in terms of detection performance.

TABLE VI. SUMMARY OF THE OVERALL DETECTION RESULTS FOR DIFFERENT ALGORITHMS OVER DIFFERENT SET OF FEATURES.

Detection rule	Set	Accuracy	Precision	Recall	F-score
Hard	S_4	81.2%	64.3%	61.3%	62.8%
Semi-hard	S_4, C/N_0, θ_{el}	86.1%	97.9%	47.2%	63.7%
Decision tree	$\mathcal{L}_1$	96.7%	93.4%	93.8%	93.6%
Decision tree	$\mathcal{L}_2$	98.0%	96.3%	96.1%	96.2%
Random forest	$\mathcal{L}_2$	99.7%	99.4%	99.3%	99.4%

2) Decision tree on set $\mathcal{L}_1$: The central row of TABLE VI reports the results obtained running the decision tree algorithm over the set of features $\mathcal{L}_1$, on the complete dataset, using a standard 10-fold cross-validation approach. The confusion matrix is reported in TABLE VII, and is the result of the average of the ten confusion matrices generated during the 10-fold cross validation process. Despite being a non standard approach, this is allowed as each fold has the same proportion of scintillation and non scintillation points.

The number of false positives and false negatives is reduced to about 3.3%. The accuracy, corresponds to 96.7%, meaning that for 164 299 over 169 955 points the machine learning prediction matches the manual annotation. The improvement, with respect to the Semi-hard rule is larger than 10%.

Complementary information is reported in Fig. 9. The figure shows the three dimensional space defined by

This article has been accepted for publication in a future issue of this journal, but has not been fully edited. Content may change prior to final publication. Citation information: DOI 10.1109/TAES.2018.2850385, IEEE Transactions on Aerospace and Electronic Systems

TABLE VII. CONFUSION MATRIX FOR THE COMPLETE DATASET USING DECISION TREE OVER SET $\mathcal{L}_1$.

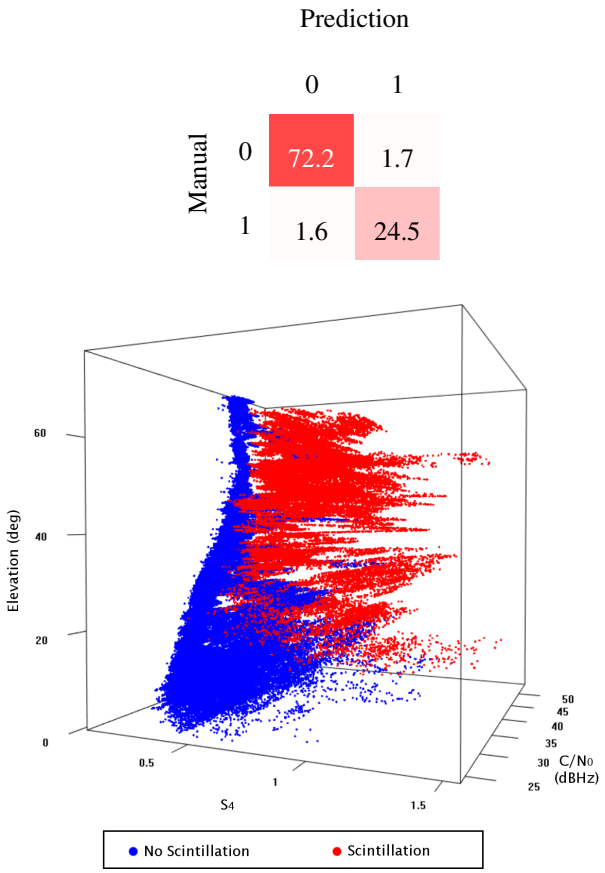

Fig. 9. Representation of the capabilities of the features defined in $\mathcal{L}_1$ to detect scintillation events.

$\mathcal{L}_1$ and reports the machine learning detection results. Blue points correspond to the portions of the signal for which no scintillation is detected, red points correspond to points for which machine learning algorithm detects scintillation. The two different regions appear to be quite well separated, sign that the global classification performance is good.

3) Decision tree on set $\mathcal{L}_2$: The last rows of TABLE VI report the results of the machine learning approaches on the set of features $\mathcal{L}_2$, identified in (13), and have been obtained performing a 10-fold cross validation.

Machine learning approaches overcome both traditional methods based on Hard and Semi-hard thresholding. The improvement, in terms of F-score, is about 30%. In addition, the signal-based set of features $\mathcal{L}_2$ outperforms the observable-based set of features $\mathcal{L}_1$. This is important, considering the fact that $\mathcal{L}_2$ only includes features obtained by averaging and summing the I and Q correlator outputs, and that more elaborated features, such as S_4 and C/N_0, are not considered. This overcomes the problem of computing the scintillation indices and in turn reduces the computational burden of the detector. No complex averaging and detrending operations are required to compute S_4 and C/N_0 values, making this approach more generic and flexible. Furthermore, the use of $\mathcal{L}_2$ makes the technique location independent, as elevation is not used.

The confusion matrix obtained averaging the 10 folds of the decision tree approach is reported in TABLE VIII. When compared to the confusion matrices for the set $\mathcal{L}_1$, the number of false positives passes from 1.7% to 1.0%, and the number of false negatives passes from from 1.6% to 1.0%.

This article has been accepted for publication in a future issue of this journal, but has not been fully edited. Content may change prior to final publication. Citation information: DOI 10.1109/TAES.2018.2850385, IEEE Transactions on Aerospace and Electronic Systems

TABLE VIII. CONFUSION MATRIX FOR THE COMPLETE DATASET USING DECISION TREE FOR SET $\mathcal{L}_2$.

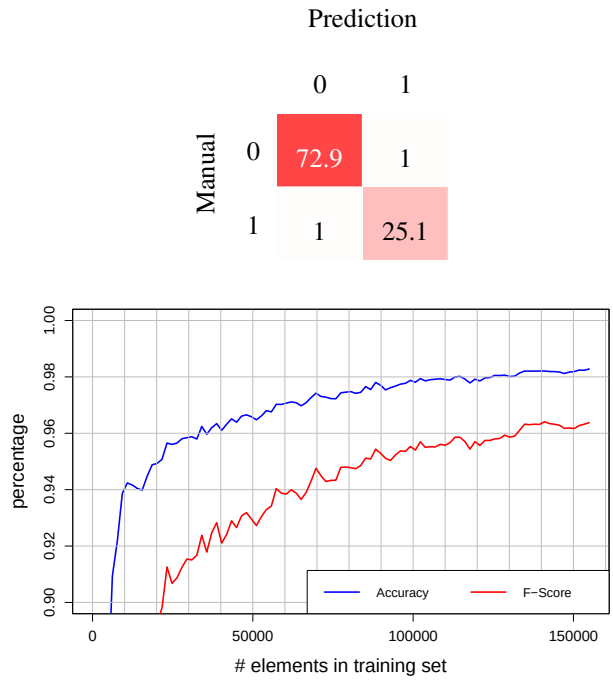

Fig. 10. Accuracy and F-score of the decision tree algorithm versus the number of points used in the training set.

Fig. 10 reports the accuracy and the F-score obtained running decision tree algorithm on set $\mathcal{L}_2$ and using 10-fold cross validation over a different number of input points. The graph shows that the value of the metrics increases as more points are used in the training phase, because the model defined by the machine learning algorithm is more complete. In order to obtain an accuracy of at least 98% and a F-score of at least 96%, a training dataset of at least 140 000 points shall be used.

TABLE VI also shows that random forest technique further improves the results, as it evaluates the decisions obtained by several decision trees, at the expenses of a higher computation burden in the training phase.

B. Qualitative analysis of the false predictions

Despite being easy to read and offering a quick quantitative overview of the overall performance of machine learning, the metrics reported in Section V-A deserve a deeper analysis. This section focuses on a few test cases, correspondent to different scintillation events, analyzing in detail the most relevant examples of false negatives and false positives. All plots show the detection results of machine learning decision tree tests, performed on set $\mathcal{L}_2$ (green points), compared to the the Hard (orange points), Semi-hard (red points) and manual/ground truth (blue points). The value of θ_{el} and of C/N_0, along with the thresholds used in the Semi-hard rule, are reported as a reference in bottom panels, for a better interpretation of the results.

First, the same two examples analyzed in Section III are reported in Fig. 11b and 11a. The detection performance of decision tree computed over set $\mathcal{L}_2$ is in line with the case over set $\mathcal{L}_1$, reported in Fig. 5. There are no false alarms, and the manual ground truth perfectly matches in both cases, confirming the goodness of the features of set $\mathcal{L}_2$.

Fig. 11c proves that the machine learning approach solves some of the the problems due to predefined

This article has been accepted for publication in a future issue of this journal, but has not been fully edited. Content may change prior to final publication. Citation information: DOI 10.1109/TAES.2018.2850385, IEEE Transactions on Aerospace and Electronic Systems

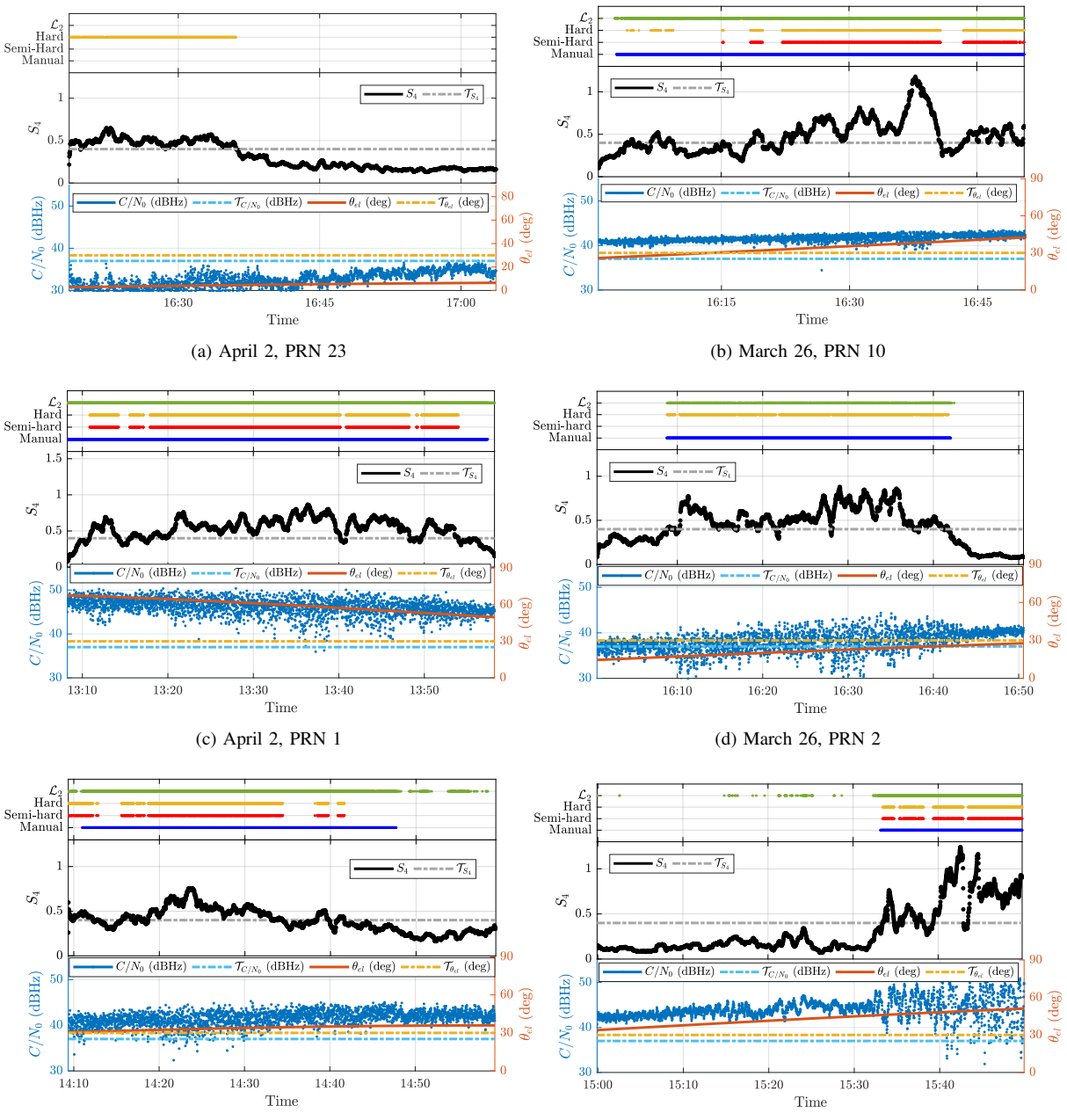

(a) April 2, PRN 23

(b) March 26, PRN 10

(c) April 2, PRN 1

(d) March 26, PRN 2

(e) April 2, PRN 3

(f) March 26, PRN 6

Fig. 11. Decision tree detection results for different test cases. Top panels report the manual annotation, the detection results of the Hard and Semi-hard rules, and the machine learning detection results, computed over set $\mathcal{L}_2$. Middle panels report the trend of the S_4 and the value of the S_4 threshold $\mathcal{T}_{S_4} = 0.4$. Bottom panels report the elevation and C/N_0 trends, and their respective thresholds used in traditional rules, $\mathcal{T}_{\theta_{\text{el}}} = 30°$ and $\mathcal{T}_{C/N_0} = 37$ dBHz.

thresholds in Hard and Semi-hard rules, thus reducing the missed detection rates and improving the overall accuracy. In this case, many points are wrongly not considered as scintillation by traditional approaches, as the value of S_4 is below $\mathcal{T}_{S_4}$. This happens both in the middle and at the borders of the event, although from visual inspection it is clear that all the points belong to the same 40-minutes long scintillation event. In particular, the raising and falling edges of the event are very well classified by machine learning with respect to Hard and Semi-hard rules. Also in this case, the decision tree prediction perfectly matches the manual annotation.

This article has been accepted for publication in a future issue of this journal, but has not been fully edited. Content may change prior to final publication. Citation information: DOI 10.1109/TAES.2018.2850385, IEEE Transactions on Aerospace and Electronic Systems

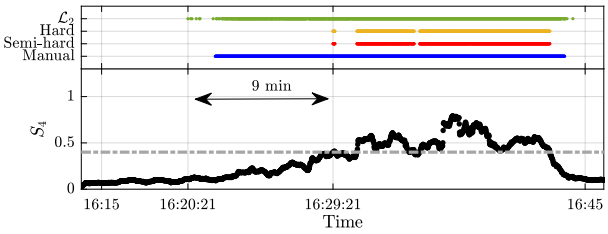

Fig. 12. Example of early scintillation detection, April 2, PRN 17.

Fig. 11d is a clear example of the importance of avoiding the a-priori filtering of data according to an elevation mask. In this case, a scintillation event can be clearly identified, despite the elevation of the satellite is below 30°. The Semi-hard rule, as well as any algorithm which applies an elevation mask to exclude low elevation satellites, would fails in detecting the event. On the contrary, the decision tree model detects the scintillation, and perfectly matches the manual annotation.

In Fig. 11e, machine learning detection gives a certain number of false positives, when compared to the manual annotation. However, a better analysis of the scintillation event could raise doubts about the correctness of the visual inspection: some of the false positives are concentrated in portions of signal for which the manual annotation could be called into question. Although the S_4 value is below the threshold, the points declared as scintillation by the decision tree algorithm could actually mark the start of a second and lighter event. Similarly, Fig. 11f reports a certain number of false alarms. Also in this case, the points in which scintillation has been detected could actually be precursors of the consecutive long event.

In general, it is possible to state that the cases in which the decision tree approach fails are not serious failures. In some cases, they correspond in ambiguous situations, and can be the consequence of carelessness in the visual inspection procedure, which is one of the limitations of human-based manual annotation. In other situations, missed detections and false alarms are isolated events, and could be completely eliminated, for instance, eliminating scintillation occurrences lasting less then a few seconds. It can be proved that an accurate post-processing of the machine learning results can lead to even higher accuracy and F-score values, further confirming the validity of the machine learning approach for autonomous scintillation detection.

C. Run time events detection

In addition to the good performance in terms of accuracy and detection rates, the results reported above show that machine learning offers a valid solution also for run time detection of the events. An increasing number of applications requires to rapidly raise an alert in case of scintillation, potentially leading to poor quality of the GNSS positioning solution. As traditional methods mostly rely on S_4, no alerts can be raised during the leading edge phase of a scintillation event. Indeed, when compared to the Hard and Semi-hard rules, decision tree approach allows an earlier detection of the event.

This is confirmed by many experimental results; one example is depicted in Fig. 12. In this specific case, machine learning can detect the scintillation event with an advance of 9 minutes, with respect to Hard and Semi-hard rules. Similar considerations could be drawn by considering the detection results reported in Fig. 11b, 11c and 11f. It is important to point out that this cannot be considered a prediction of the scintillation event, but rather an early detection. Scintillation prediction is out of the scope of this work.

This article has been accepted for publication in a future issue of this journal, but has not been fully edited. Content may change prior to final publication. Citation information: DOI 10.1109/TAES.2018.2850385, IEEE Transactions on Aerospace and Electronic Systems

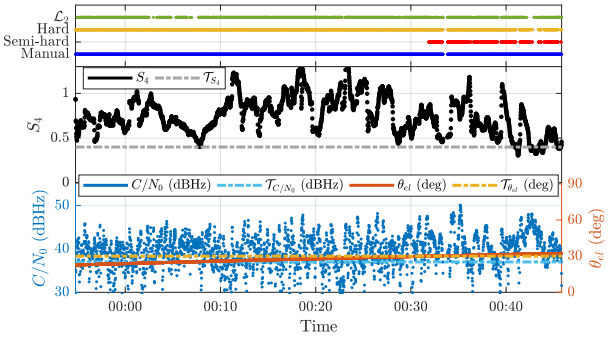

Fig. 13. Example detection for novel and untrained data, March 25, PRN 9.

D. Test on novel data

This section presents some test results on novel GNSS data affected by scintillation, in order to demonstrate the effectiveness of the decision tree approach. Data were acquired using a similar acquisition system, on March 25, 2015, in a different location (Presidente Prudente, Brasil, at a geomagentic latitude of $12^\circ\ 90'$ S). A fragment of 1 hour of data, on 7 different GPS satellites, corresponding to 28066 entries has been considered. As in the previous case, a manual ground truth has been defined by visual inspection. It is important to underline that such data are not involved in the training phase, and thus in the construction of the model. The model applied is the same considered in all previous tests, defined over the signal-based features of set $\mathcal{L}_2$.

The overall F-score is higher than 90%, while for the Semi-hard rule only 80.1% is reached. An example of detection results is reported in Fig. 13. The results for the other PRN affected by scintillation are similar and are not reported. Machine learning decision tree detection results are in line with the manual human-based annotation. All the data between 23:56 and 00:32 are below 30° of elevation. Detection techniques based on data pre-filtering would have completely discarded from the analysis the data in this interval, while rules including an elevation threshold would have wrongly marked those events as non-scintillation.

VI. Conclusion

This paper proposes a novel approach to systematically detect ionospheric scintillation events affecting the GNSS signals amplitude, characterized by a higher level of accuracy, reliability and readiness. This goal is achieved by leveraging machine learning techniques, able to learn from historical pre-classified data, and to perform automatic classification on new data. A theoretical background on GNSS, ionospheric scintillations and machine learning is given in the first part of the paper, along with a description of the classical detection techniques based on the computation of the amplitude scintillation index and on hard thresholding rules. Several tests have been carried out and are reported in Section V. The results demonstrate that this approach outperforms state-of-the art techniques in terms of accuracy and F-score, and that it can reach the levels of a manual human-driven annotation. Furthermore, it has been proven that signal based features (set $\mathcal{L}_2$) outperform observable-based features (set $\mathcal{L}_1$).

In addition, this solution offers the following added values:

1) increased generalization and location-independence, by avoiding the use of scintillation indices;
2) independence from detrending and average operations, required to compute S_4;
3) independence from a-priori filtering of data at a certain elevation mark, thus preserving potential useful information;

This article has been accepted for publication in a future issue of this journal, but has not been fully edited. Content may change prior to final publication. Citation information: DOI 10.1109/TAES.2018.2850385, IEEE Transactions on Aerospace and Electronic Systems

TABLE IX. FEATURES IDENTIFIED TO BE USED IN THE MACHINE LEARNING APPROACH.

	Name	Description
Observable-based features	S_4	The typical amplitude scintillation index used in scintillation monitoring. It is equal to zero for non-scintillation amplitude events, and increases during a scintillation event.
	C/N_0	The carrier over noise power density ratio, a low rate averaged measure of the signal strenght, based on the value of the I and Q output correlators.
	θ_{el}	The satellite's elevation angle above the horizon.
	ϑ_{az}	The satellite's azimuth with respect to the North.
Signal-based features	$\langle I \rangle$	The in-phase correlator output averaged over the observation window, defined in (6).
	$\langle Q \rangle$	The quadra-phase correlator output averaged over the observation window, defined in (7).
	$\langle I^2 \rangle$	The in-phase correlator output squared and averaged over the observation window, defined in (10).
	$\langle Q^2 \rangle$	The quadra-phase correlator output squared averaged over the observation window, defined in (11).
	$\langle SI \rangle$	The signal intensity, averaged over the observation window, defined in (9).
	$\langle SI^2 \rangle$	The signal intensity squared and averaged over the observation window, defined in (12).

4) capability to avoid false alarms due to multipath reflections;
5) improved computational speed and costs optimization in terms of human effort and time;
6) potentiality to raise early run-time scintillation alerts.

Machine learning can facilitate the work of analyzing big sets of GNSS data affected by amplitude scintillation, leading to a better understanding of the physical phenomenon, and to a potential improvement of the robustness of GNSS receivers.

APPENDIX A
SUMMARY OF ALL THE FEATURES

All the features considered in this paper are summarized in TABLE IX.

ACKNOWLEDGMENT

The authors would like to thank James T. Curran for providing an initial dataset of GNSS data affected by scintillated events and for supporting the research work with enthusiasm and with precious suggestions.

REFERENCES

[1] P. Kintner, B. Ledvina, and E. De Paula, "GPS and ionospheric scintillations," *Space weather*, vol. 5, no. 9, pp. 1–23, 2007.

[2] V. Sreeja, M. Aquino, K. de Jong, and H. Visser, "Effect of the 24 september 2011 solar radio burst on precise point positioning service," *Space Weather*, vol. 12, no. 3, pp. 143–147, 2014.

[3] B. Moreno, S. Radicella, M. C. de Lacy, M. Herraiz, and G. Rodriguez-Caderot, "On the effects of the ionospheric disturbances on precise point positioning at equatorial latitudes," *GPS Solutions*, vol. 15, no. 4, pp. 381–390, 2011.

[4] X. Zhang, F. Guo, and P. Zhou, "Improved precise point positioning in the presence of ionospheric scintillation," *GPS Solutions*, vol. 18, no. 1, pp. 51–60, 2014.

[5] J. Lee, Y. T. J. Morton, J. Lee, H.-S. Moon, and J. Seo, "Monitoring and mitigation of ionospheric anomalies for GNSS-based safety critical systems: a review of up-to-date signal processing techniques," *IEEE Signal Processing Magazine*, vol. 34, no. 5, pp. 96–110, 2017.

[6] C. Cesaroni, L. Alfonsi, R. Romero, N. Linty, F. Dovis, S. V. Veettil, J. Park, D. Barroca, M. C. Ortega, and R. O. Perez, "Monitoring ionosphere over South America: The MImOSA and MImOSA2 projects," in *International Association of Institutes of Navigation World Congress (IAIN)*, pp. 1–7, IEEE, Oct 2015.

[7] N. Linty, R. Romero, C. Cristodaro, F. Dovis, M. Bavaro, J. T. Curran, J. Fortuny-Guasch, J. Ward, G. Lamprecht, P. Riley, P. Cilliers, E. Correia, and L. Alfonsi, "Ionospheric scintillation threats to GNSS in polar regions: the DemoGRAPE case study in Antarctica," in *European Navigation Conference (ENC)*, pp. 1–7, IEEE, 2016.

[8] L. Spogli, C. Cesaroni, D. Di Mauro, M. Pezzopane, L. Alfonsi, E. Music, G. Povero, M. Pini, F. Dovis, R. Romero, N. Linty, P. Abadi, F. Nuraeni, A. Husin, M. Le Huy, T. T. Lan, T. V. La, V. G. Pillat, and N. Floury, "Formation of ionospheric irregularities over Southeast Asia during the 2015 St. Patrick's Day storm," *Journal of Geophysical Research: Space Physics*, vol. 121, no. 12, pp. 211–233, 2016.

[9] J. Vila-Valls, P. Closas, C. Fernandez-Prades, and J. T. Curran, "On the ionospheric scintillation mitigation in advanced GNSS receivers," *IEEE Transactions on Aerospace and Electronic Systems*, 2018.

[10] G. Lachapelle and A. Broumandan, "Benefits of GNSS IF data recording," in *European Navigation Conference (ENC)*, pp. 1–6, May 2016.

[11] C. Cristodaro, F. Dovis, N. Linty, and R. Romero, "Design of a configurable monitoring station for scintillations by means of a GNSS software radio receiver," *IEEE Geoscience and Remote Sensing Letters*, vol. PP, no. 99, pp. 1–5, 2018.

[12] S. Taylor, Y. Morton, Y. Jiao, J. Triplett, and W. Pelgrum, "An improved ionosphere scintillation event detection and automatic trigger for GNSS data collection systems," *2012 International Technical Meeting of The Institute of Navigation*, pp. 1563–1569, 2012.

[13] W. Fu, S. Han, C. Rizos, M. Knight, and A. Finn, "Real-time ionospheric scintillation monitoring," in *12th International Technical Meeting of the Satellite Division of The Institute of Navigation (ION GPS 1999)*, vol. 99, pp. 14–17, 1999.

[14] S. Miriyala, P. R. Koppireddi, and S. R. Chanamallu, "Robust detection of ionospheric scintillations using MF-DFA technique," *Earth, Planets and Space*, vol. 67, no. 98, pp. 1–5, 2015.

[15] R. Romero, N. Linty, F. Dovis, and R. V. Field, "A novel approach to ionospheric scintillation detection based on an open loop architecture," in *8th ESA Workshop on Satellite Navigation Technologies and European Workshop on GNSS Signals and Signal Processing (NAVITEC)*, pp. 1–9, Dec 2016.

[16] L. Rezende, E. de Paula, S. Stephany, I. Kantor, M. Muella, P. de Siqueira, and K. Correa, "Survey and prediction of the ionospheric scintillation using data mining techniques," *Space Weather*, vol. 8, no. 6, 2010.

[17] Y. Jiao, J. J. Hall, and Y. T. Morton, "Performance evaluations of an equatorial GPS amplitude scintillation detector using a machine learning algorithm," in *29th International Technical Meeting of The Satellite Division of the Institute of Navigation (ION GNSS+ 2016)*, pp. 195–199, September 2016.

[18] Y. Jiao, J. J. Hall, and Y. T. Morton, "Automatic equatorial GPS amplitude scintillation detection using a machine learning algorithm," *IEEE Transactions on Aerospace and Electronic Systems*, vol. PP, no. 99, pp. 1–1, 2017.

[19] Y. Jiao, J. J. Hall, and Y. T. Morton, "Automatic GPS phase scintillation detector using a machine learning algorithm," in *International Technical Meeting of The Institute of Navigation*, (Monterey, California), pp. 1160–1172, Janmuary 2017.

[20] Y. Jiao, J. J. Hall, and Y. T. Morton, "Performance evaluation of an automatic GPS ionospheric phase scintillation detector using a machine-learning algorithm," *Navigation*, vol. 64, no. 3, pp. 391–402, 2017.

[21] P. W. Ward, J. W. Betz, and C. J. Hegarty, "Satellite signal acquisition, tracking, and data demodulation," in *Understanding GPS: principles and applications* (A. House, ed.), pp. 153–241, Kaplan, E. and Hegarty, C., 2006.

[22] A. Van Dierendonck, J. Klobuchar, and Q. Hua, "Ionospheric scintillation monitoring using commercial single frequency C/A code receivers," in *6th International Technical Meeting of the Satellite Division of The Institute of Navigation (ION GPS 1993)*, vol. 93, (Salt Lake City, UT), pp. 1333–1342, September 1993.

[23] P. Flach, *Machine learning: the art and science of algorithms that make sense of data*. Cambridge University Press, 2012.

[24] A. Favenza, N. Linty, and F. Dovis, "Exploiting standardized metadata for GNSS SDR remote processing: a case study," in *29th International Technical Meeting of The Satellite Division of the Institute of Navigation (ION GNSS+ 2016)*, (Portland, Oregon), pp. 77–85, September 2016.

[25] T. M. Mitchell, *Machine learning*. McGraw Hill, 1997.

[26] J. R. Quinlan, "Induction of decision trees," *Machine learning*, vol. 1, no. 1, pp. 81–106, 1986.

[27] R. Tibshirani and J. Friedman, *The elements of statistical learning: data mining, inference, and prediction*. Springer, 2001.

[28] N. Japkowicz and M. Shah, *Evaluating learning algorithms: a classification perspective*. Cambridge University Press, 2011.

[29] L. Breiman, "Random forests," *Machine learning*, vol. 45, no. 1, pp. 5–32, 2001.

[30] P. Refaeilzadeh, L. Tang, and H. Liu, "Cross-validation," in *Encyclopedia of database systems*, pp. 532–538, Springer, 2009.

[31] S. Dubey, R. Wahi, E. Mingkhwan, and A. Gwal, "Study of amplitude and phase scintillation at GPS frequency," *94.20. S; 94.20. J*, 2005.

[32] E. Aon, A. R. Othman, Y. H. Ho, and R. Shaddad, "A study of ionospheric GPS scintillation during solar maximum at UTeM station," *Jurnal Teknologi*, pp. 123–128, 2015.

[33] R. M. Romero Gaviria, *Estimation Techniques and Mitigation Tools for Ionospheric effects on GNSS Receivers*. PhD thesis, Politecnico di Torino, 2015.

[34] R. W. Middlestead, *Digital Communications with Emphasis on Data Modems: Theory, Analysis, Design, Simulation, Testing, and Applications*. John Wiley & Sons, 2017.

[35] A. Adewale, E. Oyeyemi, A. Adeloye, C. N. Mitchell, J. A. Rose, and P. Cilliers, "A study of L-band scintillations and total electron content at an equatorial station, Lagos, Nigeria," *Radio Science*, vol. 47, no. 2, 2012.

[36] Y. Jiao, Y. T. Morton, S. Taylor, and W. Pelgrum, "Characterization of high-latitude ionospheric scintillation of GPS signals," *Radio Science*, vol. 48, no. 6, pp. 698–708, 2013.

[37] P. Abadi, S. Saito, and W. Srigutomo, "Low-latitude scintillation occurrences around the equatorial anomaly crest over Indonesia," *Annales Geophysicae*, vol. 32, no. 1, pp. 7–17, 2014.

[38] J. T. Curran, M. Bavaro, A. Morrison, and J. Fortuny, "Developing a multi-frequency for GNSS-based scintillation monitoring receiver," in *27th International Technical Meeting of The Satellite Division of the Institute of Navigation (ION GNSS+ 2014)*, (Tampa, Florida), pp. 1142–1152, September 2014.

[39] M. Najmafshar, S. Skone, and F. Ghafoori, "GNSS data processing investigations for characterizing ionospheric scintillation," in *27th International Technical Meeting of The Satellite Division of the Institute of Navigation (ION GNSS+ 2014)*, (Tampa, Florida), pp. 1190–1202, September 2014.

[40] M. H. Mokhtar, *Mitigation of scintillation effects on GPS satellite positioning*. PhD thesis, University of Leeds, 2012.

[41] S. C. Mushini, P. Jayachandran, R. Langley, J. MacDougall, and D. Pokhotelov, "Improved amplitude-and phase-scintillation indices derived from wavelet detrended high-latitude GPS data," *GPS solutions*, vol. 16, no. 3, pp. 363–373, 2012.

[42] F. Niu, *Performances of GPS signal observables detrending methods for ionosphere scintillation studies*. PhD thesis, Miami University, 2012.

[43] B. Forte and S. M. Radicella, "Problems in data treatment for ionospheric scintillation measurements," *Radio Science*, vol. 37, no. 6, 2002.

[44] R. Taylor, "Interpretation of the correlation coefficient: a basic review," *Journal of diagnostic medical sonography*, vol. 6, no. 1, pp. 35–39, 1990.

[45] A. Favenza, A. Farasin, N. Linty, and F. Dovis, "A machine learning approach to GNSS scintillation detection: automatic soft inspection of the events," in *30th international technical meeting of the satellite division of the institute of navigation (ION GNSS+ 2017)*, pp. 4103–4111, September 2017.

[46] T. Y. Atilaw, P. Cilliers, and P. Martinez, "Azimuth-dependent elevation threshold (ADET) masks to reduce multipath errors in ionospheric studies using GNSS," *Advances in Space Research*, vol. 59, no. 11, pp. 2726–2739, 2017.

This article has been accepted for publication in a future issue of this journal, but has not been fully edited. Content may change prior to final publication. Citation information: DOI 10.1109/TAES.2018.2850385, IEEE Transactions on Aerospace and Electronic Systems

Nicola Linty is an assistant professor at the Department of Electronics and Telecommunications (DET) of Politecnico di Torino (Italy), and member of the NavSAS research group. His research interests cover the field of signal processing and simulation, applied to satellite navigation. In particular, his work deals with the design and development of innovative algorithms for GPS and Galileo receivers.

Alessandro Farasin is a researcher and software developer at Istituto Superiore Mario Boella in Turin. He is a PhD student at Department of Automation and Informatics (DAUIN) the Politecnico of Torino (Italy) as well. In 2016, he graduated with honors in Computer Science at Università degli Studi di Torino. He is working at the Microsoft Innovation Center area of ISMB, architecting and developing solutions based on Microsoft technologies, mainly focused on cloud, big data and machine learning related topics. His PhD studies are mainly focused on Machine Learning algorithms, exploited and realized for the analysis of Geospatial data.

Alfredo Favenza is a senior researcher and project manager at Istituto Superiore Mario Boella in Turin. In 2007, he received his Master of Science in Computer Science and started his research activity in ISMB in the area of Navigation technologies developing strong expertise on GNSS Software Defined Radio, and Augmentation Systems (EGNOS/EDAS). Nowadays, Alfredo is a researcher of Mobile Solutions Research Area of ISMB interested in cross-technologies domains where Location-Based services, Big Data and Navigation technologies can be combined to generate added-value innovation.

Fabio Dovis is an associate professor at the Department of Electronics and Telecommunications of Politecnico di Torino as a member of the Navigation Signal Analysis and Simulation (NavSAS) group. His research interests cover the design of GPS and Galileo receivers and advanced signal processing for interference and multipath detection and mitigation. He has a relevant experience in European projects in satellite navigation as well as cooperation with industries and research centers.